Journal of Applied and Numerical Analysis
2026, Vol. 4, pp. 235–251
doi: 10.30970/ana.2026.4.6

A robust h-adaptive finite element method with multiple element subdivision for cylindrical shell boundary value problems

Heorhiy Shynkarenko[1], Pavlo Malashnyak[1,*], Vitaliy Horlatch[1]

[1] *Faculty of Applied Mathematics and Informatics, Ivan Franko National University of Lviv, 1 Universytetska St, Lviv, 79000, Ukraine*

Анотація. У статті побудовано алгоритм h-адаптивного МСЕ з поелементно визначеним апостеріорним оцінювачем похибок залишкового гатунку, заснований на рекурентному покращенні наближень до шуканого розв'язку із заздалегідь заданою точністю. Система керування процесом базується на аналізі значень індикаторів апостеріорного оцінювача похибок кожного скінченного елемента та критерію його багатократного подрібнення з метою досягнення рівномірного розподілу похибок між складниками сітки. Спираючись на задану максимально допустиму кількість поділів елемента, наводяться числові результати обчислювальних експериментів з сингулярно збуреною задачею з примежовими шарами в околах защемлених торців оболонки. Стаття містить детальний аналіз збіжності апроксимацій на локально згущуваних сітках з використанням енергетичної норми, що демонструє надійність та ефективність (тобто добротність) сконструйованої схеми h-адаптивного МСЕ та її здатність відтворювати істинні розв'язки з високою достовірністю.

Abstract. This article is devoted to the construction of an h-adaptive FEM algorithm with an element-by-element a posteriori error estimator of the residual type, which is based on the iterative improvement of approximations to the desired solution with a predefined accuracy. The process control system is based on the analysis of the values of the a posteriori error estimator indicators for each finite element and the criterion of its multiple refinement, with the aim of achieving a uniform distribution of errors among the grid components. Based on a given maximum permissible number of element subdivisions, we present numerical results of our computational experiments with singularly perturbed problems caused by the presence of boundary layers in the neighborhood of clamped shell ends. The remainder of the article contains a detailed analysis of the convergence of approximations on locally refined meshes using equivalent norms of the space of admissible displacements, demonstrating the efficiency and reliability of the constructed h-adaptive FEM scheme and its ability to reproduce the true errors of the approximations with high accuracy.

1 Introduction

The pioneering work [3] laid the foundation in the theory and practice of the finite element method for a fruitful line of research, which over time supplemented its algorithms with a posteriori error estimators (AEE) for computed approximations, as well as various adaptive versions aimed

* Corresponding author: pavlo.malashnyak@lnu.edu.ua
Key words: h-adaptive finite element method, cylindrical shell, a posteriori error estimator, Timoshenko model, singular perturbation, multiple element subdivision.
© Shynkarenko H., Malashnyak P., Horlatch V., 2026

at finding approximate solutions with a pre-specified permissible error and minimal computational cost. The main results of these studies can be found in the monographs [2, 4, 5, 14, 16, 17], early reviews [11, 15] and the recently updated survey [6], all of which contain extensive lists of references to original journal and conference contributions. Such finite element schemes have proven particularly valuable in the numerical analysis of singularly perturbed boundary value problems, whose solutions have little stability margin and therefore often require excessive computational effort. A wide class of applied problems of this type includes problems of continuum mechanics and physics, in particular, the statics and harmonic vibrations of Timoshenko shells [9, 10].

In this context, the main objective of our studies is to develop, for the Timoshenko cylindrical shell model, a control system for the recursive process of computing a convergent sequence of finite element approximations, which optimises computational costs by improving mesh resolution solely through localised multiple subdivision of selected finite elements. To this end, in Section 1 we introduce the Timoshenko cylindrical shell boundary value problem. Section 2 presents the variational formulation of the static equilibrium problem for a thin Timoshenko cylindrical shell and its FEM discretisation for finding the piecewise linear approximation of the vector of generalised displacements. Section 3 is devoted to the residual problem of the found finite element approximation and its piecewise quadratic solution on the running finite element mesh, which is subsequently used as the a posteriori error estimator for this approximation. We present in detail the procedure for computing the contributions (indicators) to this AEE from each finite element of the mesh which generalises the methodology of [1] to the case of vector-valued functions. The analytically computed expansion coefficients of the indicators show that they are proportional to the squares of the finite element lengths. Section 4 presents certain convergence characteristics of the sequence of finite element approximations and their AEEs, computed on a sequence of nested spaces, as well as tools for evaluating the quality of the found approximations. Section 5 is devoted to a description of the recursive adaptation algorithm (solve, estimate, mark and refine), whose distinctive feature is a control mechanism based on the parameter of the maximum permissible subdivision of a finite element [8]. The analysis of numerical experiments, carried out in Section 6 on the example of a shell with boundary layers in the neighborhood of its rigidly clamped ends, uses efficiency indices to confirm the reliability and efficiency of the proposed AEE and the h-adaptive computational scheme for achieving approximations with a pre-specified error tolerance and minimal computational cost. The conclusions in Section 7 summarise the obtained results.

2 Timoshenko cylindrical shell boundary value problem

We consider an axisymmetric static equilibrium problem for a homogeneous isotropic circular cylindrical shell of radius R, length L and thickness $t > 0$, $t/R \le 1$: find the vector of generalised elastic displacements $\boldsymbol{\psi}(z) = [u(z), w(z), \gamma(z)]^T$, the strain tensor components $\boldsymbol{\varepsilon} = [\varepsilon_1, \varepsilon_2, \varepsilon_{13}, \varkappa_1]^T$ and the stress resultants $\boldsymbol{\sigma} = [N_u, N_w, N_{13}, M_\gamma]^T$, satisfying the equilibrium equations

$$-\frac{d}{dz}N_u = f_u, \qquad -\frac{d}{dz}N_{13} + R^{-1}N_w = f_w, \qquad -\frac{d}{dz}M_\gamma + N_{13} = f_\gamma \quad \text{in } \Omega = (0, L), \tag{2.1}$$

Hooke's law $\boldsymbol{\sigma} = \mathbf{K}\boldsymbol{\varepsilon}$, i.e.

$$\begin{bmatrix} N_u \\ N_w \\ N_{13} \\ M_\gamma \end{bmatrix} = \begin{bmatrix} B & \nu B & 0 & 0 \\ \nu B & B & 0 & 0 \\ 0 & 0 & B_c & 0 \\ 0 & 0 & 0 & D \end{bmatrix} \begin{bmatrix} \varepsilon_1 \\ \varepsilon_2 \\ \varepsilon_{13} \\ \varkappa_1 \end{bmatrix} \quad \text{in } \Omega = (0, L), \tag{2.2}$$

the Cauchy relations $\boldsymbol{\varepsilon} = \mathbf{C}\boldsymbol{\psi}$, i.e.

$$\begin{bmatrix} \varepsilon_1 \\ \varepsilon_2 \\ \varepsilon_{13} \\ \varkappa_1 \end{bmatrix} = \begin{bmatrix} \frac{d}{dz} & 0 & 0 \\ 0 & \frac{1}{R} & 0 \\ 0 & \frac{d}{dz} & 1 \\ 0 & 0 & \frac{d}{dz} \end{bmatrix} \begin{bmatrix} u \\ w \\ \gamma \end{bmatrix} \quad \text{in } \Omega = (0, L), \tag{2.3}$$

and the clamped–clamped boundary conditions

$$\boldsymbol{\psi}(0) = \mathbf{0}, \qquad \boldsymbol{\psi}(L) = \mathbf{0}. \tag{2.4}$$

The stiffness coefficients are determined by

$$B = \frac{Et}{1-\nu^2}, \quad D = \frac{Et^3}{12(1-\nu^2)}, \quad B_c = \frac{5Et}{12(1+\nu)}, \tag{2.5}$$

where $E > 0$ and $\nu \in (0, \frac{1}{2})$ are the Young's modulus and Poisson's ratio of the shell material of radius R, length L and thickness $t > 0$; $\mathbf{f}(z) = \{f_u(z), f_w(z), f_\gamma(z)\}$ is the given surface load vector.

Substituting (2.2)–(2.3) into (2.1)–(2.4) yields the second-order matrix differential equation

$$-\mathbf{A}\boldsymbol{\psi}'' + \mathbf{G}\boldsymbol{\psi}' + \mathbf{S}\boldsymbol{\psi} = \mathbf{f}(z) \quad \text{in } \Omega, \tag{2.6}$$

where

$$\mathbf{A} = \begin{bmatrix} B & 0 & 0 \\ 0 & B_c & 0 \\ 0 & 0 & D \end{bmatrix}, \quad \mathbf{G} = \begin{bmatrix} 0 & -\nu R^{-1} B & 0 \\ \nu R^{-1} B & 0 & -B_c \\ 0 & B_c & 0 \end{bmatrix}, \quad \mathbf{S} = \begin{bmatrix} 0 & 0 & 0 \\ 0 & R^{-2} B & 0 \\ 0 & 0 & B_c \end{bmatrix},$$

with the clamped-clamped boundary conditions (2.4).

The positive definite diagonal matrix $\mathbf{A} = \operatorname{diag}[B, B_c, D]$ ensures unique solvability of (2.4), (2.6) for the higher derivatives and thus for the solution $\boldsymbol{\psi}$.

3 Problem formulation and notation

We consider a variational problem concerning the stress state of a rigidly clamped circular cylindrical shell under an axisymmetric load, which, in the terms of the paper [12] within the framework of the Timoshenko model ($t > 0$, $\frac{t}{R} \ll 1$), is described as follows:

Given the meridian length L, the radius R and the shell thickness t, as well as its stiffness coefficients B, B_c, D and the surface load vector $\mathbf{f} = \{f_u, f_w, f_\gamma\}$;

find the vector of generalised displacements

$$\boldsymbol{\psi} = \{u, w, \gamma\} \in \Phi := \Big\{ \boldsymbol{\varphi} = \{v, y, \xi\} \in \big[H^1((0, L))\big]^3 : \ \boldsymbol{\varphi}(0) = 0, \boldsymbol{\varphi}(L) = 0 \Big\}$$

such that it satisfies the equation

$$\Pi(\boldsymbol{\psi}, \boldsymbol{\varphi}) = \langle l, \boldsymbol{\varphi} \rangle \quad \forall\, \boldsymbol{\varphi} \in \Phi, \tag{3.1}$$

where

$$\begin{aligned} \Pi(\boldsymbol{\psi}, \boldsymbol{\varphi}) := & \int_0^L B\big[(u'v' + R^{-2}wy) + \nu R^{-1}(wv' + u'y)\big]\, dz \\ & + \int_0^L \big[B_c(w' + \gamma)(y' + \xi) + D\gamma'\xi'\big]\, dz, \quad \forall\, \boldsymbol{\psi}, \boldsymbol{\varphi} \in \Phi, \end{aligned} \tag{3.2}$$

$$\langle l, \boldsymbol{\varphi} \rangle := \int_0^L (f_u v + f_w y + f_\gamma \xi)\, dz \quad \forall\, \boldsymbol{\varphi} \in \Phi. \tag{3.3}$$

For the physical interpretation of the stiffness parameters B, B_c, D and the surface load vector $\mathbf{f}$ entering the bilinear form (3.2)–(3.3), see [2]. In the article [12], it is shown that the problem (3.1)–(3.3) has a unique solution $\boldsymbol{\psi} \in \Phi$, which depends continuously on its data in the energy norm of the space of admissible displacements Φ:

$$\|\boldsymbol{\varphi}\|_\Pi := \Pi^{1/2}(\boldsymbol{\varphi}, \boldsymbol{\varphi}) \quad \forall\, \boldsymbol{\varphi} \in \Phi.$$

Throughout the remainder of this paper, we assume that on the finite element mesh $\mathcal{T}_h = \{K_{i+1/2}\}_{i=0}^{N-1}$ with nodes $0 = z_0 < z_1 < \ldots < z_N = L$, $K_{i+1/2} := (z_i, z_{i+1})$, scalar piecewise linear functions $\varphi_i = \varphi_i(z)$, $i = 1, \ldots, N$, have been constructed, which satisfy the property $\varphi_i(z_j) = \delta_{ij}$, where δ is the Kronecker delta. Hereinafter, we use the notations: $h_{i+1/2} = |K_{i+1/2}| = z_{i+1} - z_i$, $h = \max_{K_{i+1/2} \in \mathcal{T}_h} h_{i+1/2}$.

The standard finite element procedure for solving problem (3.1)–(3.3) leads to finding its approximate solution from the discrete analogue of the problem:

Given that

$$\Phi_h := \operatorname{span}\left[\left\{ \begin{pmatrix} \varphi_i \\ 0 \\ 0 \end{pmatrix}, \begin{pmatrix} 0 \\ \varphi_i \\ 0 \end{pmatrix}, \begin{pmatrix} 0 \\ 0 \\ \varphi_i \end{pmatrix} \right\}_{i=1}^{N-1} \right] \subset \Phi;$$

find $\boldsymbol{\psi}_h \in \Phi_h$ *such that*

$$\Pi(\boldsymbol{\psi}_h, \boldsymbol{\varphi}) = \langle l, \boldsymbol{\varphi} \rangle \quad \forall\, \boldsymbol{\varphi} \in \Phi_h. \tag{3.4}$$

In addition to the usual presentation of numerical simulation results in the form of tables, we supplement these with approximate error estimates based on a posteriori error estimators (AEE).

4 Residual a posteriori error estimator

In the paper [13], an a posteriori error estimator $\boldsymbol{\varepsilon}_h \in E_h \subset \Phi \setminus \Phi_h$ is constructed for the found approximation $\boldsymbol{\psi}_h \in \Phi_h$ on the following principles of computational minimisation:

(i) the determination of the AEE is tied to the running grid $\mathcal{T}_h = \{K_{i+1/2}\}_{i=0}^{N-1}$ such that

$$\boldsymbol{\varepsilon}_h(z) := \sum_{i=0}^{N-1} \boldsymbol{\varepsilon}_{i+1/2}(z), \quad \operatorname{supp} \boldsymbol{\varepsilon}_{i+1/2} = K_{i+1/2},$$

therefore, the AEE indicators $\boldsymbol{\varepsilon}_{i+1/2}$ can be calculated at each $K_{i+1/2}$ independently of the remaining finite elements of the mesh;

(ii) each indicator $\boldsymbol{\varepsilon}_{i+1/2}$ is described at $K_{i+1/2}$ by a linear combination of basis vectors $\{\mathbf{b}_j(z)\}$ of the form

$$\begin{aligned} \boldsymbol{\varepsilon}_{i+1/2}(z) &= \lambda_u\, \mathbf{b}_1(z) + \lambda_w\, \mathbf{b}_2(z) + \lambda_\gamma\, \mathbf{b}_3(z) \\ &= \lambda_u \begin{bmatrix} b_{i+1/2}(z) \\ 0 \\ 0 \end{bmatrix} + \lambda_w \begin{bmatrix} 0 \\ b_{i+1/2}(z) \\ 0 \end{bmatrix} + \lambda_\gamma \begin{bmatrix} 0 \\ 0 \\ b_{i+1/2}(z) \end{bmatrix}, \quad \forall z \in K_{i+1/2}, \end{aligned} \tag{4.1}$$

where the coefficients $\boldsymbol{\lambda}_{i+1/2} = [\lambda_u, \lambda_w, \lambda_\gamma]^T \in \mathbb{R}^3$ are to be determined;

(iii) the orthogonality of the indicator basis vectors is complemented by a generating (bubble) function $b_{i+1/2} = b_{i+1/2}(z)$, which is a quadratic polynomial

$$b_{i+1/2}(z) := 4\,\frac{z_{i+1}-z}{h_{i+1/2}}\cdot\frac{z-z_i}{h_{i+1/2}}, \quad \operatorname{supp} b_{i+1/2} = K_{i+1/2} = (z_i, z_{i+1}), \tag{4.2}$$

with the properties: $b_{i+1/2}(z_i) = b_{i+1/2}(z_{i+1}) = 0$; $b_{i+1/2}\Big(\frac{z_i+z_{i+1}}{2}\Big) = 1$.

Given (i)–(iii), it is easy to see that the sought-after coefficients $\boldsymbol{\lambda}_{i+1/2}$ of the AEE indicator represent approximate values of the approximation error of the vector of generalised displacements at the centre $z_{i+1/2} = \frac{z_i+z_{i+1}}{2}$ of the finite element $K_{i+1/2}$; in other words:

$$\boldsymbol{\varepsilon}_{i+1/2}(z_m) = \boldsymbol{\lambda}_{i+1/2} \cong \boldsymbol{\psi}(z_m) - \boldsymbol{\psi}_h(z_m), \quad m = i + \tfrac{1}{2}.$$

The aforementioned coefficients of the indicator $\boldsymbol{\lambda}_{i+1/2} \in \mathbb{R}^3$ are calculated from the variational equations of the residual of the found approximation $\boldsymbol{\psi}_h \in \Phi_h$:

$$\Pi(\boldsymbol{\varepsilon}_{i+1/2}, \mathbf{b}_m) = \langle \mathcal{R}_{i+1/2}, \mathbf{b}_m\rangle := \langle l, \mathbf{b}_m\rangle - \Pi(\boldsymbol{\psi}_h, \mathbf{b}_m), \quad m = 1, 2, 3. \tag{4.3}$$

Hence, due to the orthogonality of $\{\mathbf{b}_j(z)\}$, we obtain that

$$\boldsymbol{\lambda}_{i+1/2} = [\lambda_u, \lambda_w, \lambda_\gamma]^T = \left[\frac{\langle \mathcal{R}_{i+1/2}, \mathbf{b}_1\rangle}{\Pi(\mathbf{b}_1, \mathbf{b}_1)}, \frac{\langle \mathcal{R}_{i+1/2}, \mathbf{b}_2\rangle}{\Pi(\mathbf{b}_2, \mathbf{b}_2)}, \frac{\langle \mathcal{R}_{i+1/2}, \mathbf{b}_3\rangle}{\Pi(\mathbf{b}_3, \mathbf{b}_3)}\right]^T,$$

or, after analytical calculations,

$$\begin{aligned}
\lambda_u &= \frac{h^2}{8}\,\frac{f_u + \nu R^{-1} B\dfrac{w_{i+1}-w_i}{h}}{B},\\
\lambda_w &= \frac{h^2}{8}\,\frac{f_w - \dfrac{B}{R}\left(\dfrac{w_{i+1}+w_i}{2R} + \nu\dfrac{u_{i+1}-u_i}{h}\right) + B_c\dfrac{\gamma_{i+1}-\gamma_i}{h}}{B_c + \dfrac{1}{10}BR^{-2}h^2},\\
\lambda_\gamma &= \frac{h^2}{8}\,\frac{f_\gamma - B_c\left(\dfrac{w_{i+1}-w_i}{h} + \dfrac{\gamma_{i+1}+\gamma_i}{2}\right)}{D + \dfrac{1}{10}B_c h^2},
\end{aligned} \tag{4.4}$$

where we adopt the notation $h \equiv h_{i+1/2}$, $g_m = g(z_m)$, and

$$\begin{aligned}
\Pi_{11} &= \Pi(\mathbf{b}_1, \mathbf{b}_1) \cong \tfrac{16}{3}h_{i+1/2}^{-1}B,\\
\Pi_{22} &= \Pi(\mathbf{b}_2, \mathbf{b}_2) \cong \tfrac{16}{3}h_{i+1/2}^{-1}B_c + \tfrac{8}{15}h_{i+1/2}BR^{-2},\\
\Pi_{33} &= \Pi(\mathbf{b}_3, \mathbf{b}_3) \cong \tfrac{16}{3}h_{i+1/2}^{-1}D + \tfrac{8}{15}h_{i+1/2}B_c,\\
\langle \mathcal{R}_{i+1/2}, \mathbf{b}_1\rangle &\cong \tfrac{2}{3}h_{i+1/2}\left[f_u + \nu R^{-1}B\frac{w_{i+1}-w_i}{h}\right],\\
\langle \mathcal{R}_{i+1/2}, \mathbf{b}_2\rangle &\cong \tfrac{2}{3}h_{i+1/2}\left[f_w - BR^{-1}(R^{-1}w_{i+1/2} + \nu\frac{u_{i+1}-u_i}{h}) + B_c\frac{\gamma_{i+1}-\gamma_i}{h}\right],\\
\langle \mathcal{R}_{i+1/2}, \mathbf{b}_3\rangle &\cong \tfrac{2}{3}h_{i+1/2}\left[f_\gamma - B_c(\gamma_{i+1/2} + \frac{w_{i+1}-w_i}{h})\right].
\end{aligned}$$

Thus, on each finite element $K_{i+1/2} \in \mathcal{T}_h$, the AEE is described solely by the values of the indicator $\boldsymbol{\varepsilon}_{i+1/2} = \boldsymbol{\varepsilon}_{i+1/2}(z)$, which is defined in (4.1), (4.2) and (4.4). Its magnitude is characterised by the energy norm

$$\theta^2_{i+1/2} := \|\boldsymbol{\varepsilon}_{i+1/2}\|^2_\Pi = \Pi_{11}\lambda_u^2 + \Pi_{22}\lambda_w^2 + \Pi_{33}\lambda_\gamma^2 = \langle \mathcal{R}_{i+1/2}, \mathbf{b}_1\rangle\lambda_u + \langle \mathcal{R}_{i+1/2}, \mathbf{b}_2\rangle\lambda_w + \langle \mathcal{R}_{i+1/2}, \mathbf{b}_3\rangle\lambda_\gamma.$$

By summing the indicators over all finite elements of the partition, we find the energy norm of the AEE:

$$\eta_h^2 := \|\boldsymbol{\varepsilon}_h\|^2_\Pi \equiv \sum_{i=0}^{N-1} \theta^2_{i+1/2}.$$

Note here that the solutions to equations (4.3) determine, at each $K_{i+1/2}$, the best approximations to the true error in terms of the energy norm. Naturally, their quality depends on the choice of basis functions $\{\mathbf{b}_j(z)\}$.

5 Quality criteria for the found approximation

In the paper [13], it is shown that the sequence of approximate solutions $\{\boldsymbol{\psi}_n\}_{n\geq 0} \subset \Phi$ to problems (3.1)–(3.4) will converge to its solution $\boldsymbol{\psi} \in \Phi$, if these approximations are computed using a corresponding sequence of nested spaces $\{\Phi_n\}_{n\geq 0} \subset \Phi$, $\Phi_n \subset \Phi_{n+1}$, such that the union $\cup_{n\geq 0}\Phi_n$ is a dense (in the sense of the energy norm $\|\cdot\|_\Pi$) subspace of the space Φ. Having computed the corresponding sequence of AEEs $\{\boldsymbol{\varepsilon}_n\}_{n\geq 0}$ in accordance with Section 2, we can use the following estimates for the approximations found with any $n \geq 0$:

(i) $\|\boldsymbol{\psi}_n\|_\Pi \leq \|\boldsymbol{\psi}\|_\Pi$;

(ii) $\|\boldsymbol{\psi}_{n+1} - \boldsymbol{\psi}_n\|_\Pi = \left(\|\boldsymbol{\psi}_{n+1}\|^2_\Pi - \|\boldsymbol{\psi}_n\|^2_\Pi\right)^{1/2} \leq \left(\|\boldsymbol{\psi}\|^2_\Pi - \|\boldsymbol{\psi}_n\|^2_\Pi\right)^{1/2} = \|\boldsymbol{\psi} - \boldsymbol{\psi}_n\|_\Pi$;

(iii) $\|\boldsymbol{\varepsilon}_n\|_\Pi \leq \|\boldsymbol{\psi} - \boldsymbol{\psi}_n\|_\Pi$.

Based on these absolute error estimates, we can calculate:

(i) *the relative errors*

$$\delta_n := \frac{\|\boldsymbol{\varepsilon}_n\|_\Pi}{\|\boldsymbol{\psi}_n\|_\Pi}100\%, \quad r_n := \frac{\|\boldsymbol{\psi} - \boldsymbol{\psi}_n\|_\Pi}{\|\boldsymbol{\psi}_n\|_\Pi}100\%, \quad \eta_n := \frac{\|\boldsymbol{\psi}_{n+1} - \boldsymbol{\psi}_n\|_\Pi}{\|\boldsymbol{\psi}_n\|_\Pi}100\%; \tag{5.1}$$

(ii) *the convergence orders of* the error approximations

$$p_n := \frac{\ln\|\boldsymbol{\varepsilon}_{n-1}\|_\Pi - \ln\|\boldsymbol{\varepsilon}_n\|_\Pi}{\ln[\mathrm{card}(\mathcal{T}_n)] - \ln[\mathrm{card}(\mathcal{T}_{n-1})]}, \tag{5.2}$$

where $\mathrm{card}(\mathcal{T}_n)$ is the number of finite elements of the mesh $\mathcal{T}_n$ used to construct the space Φ_n;

(iii) *the non-uniformity of the finite element mesh*

$$\chi_n := \frac{\max_{K\in\mathcal{T}_n} h_K}{\min_{K\in\mathcal{T}_n} h_K}, \tag{5.3}$$

which may signal a deterioration in stability of calculations on irregular partitions;

(iv) *the estimator efficiency index*

$$I_n := \frac{\|\boldsymbol{\psi} - \boldsymbol{\psi}_n\|_\Pi}{\|\boldsymbol{\varepsilon}_n\|_\Pi} \geq 1, \tag{5.4}$$

which indicates how close the AEE estimates are to the true error values and allows the calculation of two-sided error estimates (AEE quality) via the following formula:

$$\frac{I_n}{2I_n - 1}\|\boldsymbol{\varepsilon}_n\|_\Pi \leq \|\boldsymbol{\psi} - \boldsymbol{\psi}_n\|_\Pi \leq I_n\|\boldsymbol{\varepsilon}_n\|_\Pi; \tag{5.5}$$

(v) *the distribution of local quality characteristics*

$$\omega_{i+1/2} := \frac{\|\boldsymbol{\varepsilon}_{i+1/2}\|_\Pi \sqrt{N}}{\|\boldsymbol{\psi}_h\|_\Pi} 100\% \quad \forall\, K_{i+1/2} \in \mathcal{T}_h, i = 1, \ldots, N.$$

6 Recurrent algorithm for solving with pre-specified accuracy

Our aim is to construct an algorithm that allows us to determine an efficient multiple subdivision of a given finite element in such a way as to reduce the computational cost of finding an approximation to the solution of the problem with pre-specified requirements for the permissible approximation error, more precisely:

a permissible error level tol (%) *is given*;

find a partition $\mathcal{T}^* = \{K\}$ *of the interval* $\Omega = [0, L] \subset \mathbb{R}$ *and a corresponding piecewise linear basis* $\mathcal{B}^* = \{\mathbf{b}_i\}$ *of the finite-dimensional subspace* $\Phi^* \subset \Phi$ *such that the piecewise linear finite element approximation* $\boldsymbol{\psi}^* \in \Phi^* \subset \Phi$*, computed with reduced computational cost, is a solution to the equation*

$$\Pi(\boldsymbol{\psi}^*, \boldsymbol{\varphi}) = \langle l, \boldsymbol{\varphi} \rangle \quad \forall\, \boldsymbol{\varphi} \in \Phi^*$$

and satisfies an additional condition regarding the accuracy of the approximation

$$\frac{\|\boldsymbol{\psi} - \boldsymbol{\psi}^*\|_\Pi}{\|\boldsymbol{\psi}^*\|_\Pi} 100\% \le tol, \tag{6.1}$$

where $\boldsymbol{\psi} \in \Phi$ *is the sought solution to the variational problem* (3.1)–(3.3).

The recursive algorithm proposed below for solving the optimisation problem (6.1) comprises the following steps:

1. *a permissible level of approximation error* $tol > 0$*, an initial grid* $\mathcal{T}_0 = \{K\}$*, and a subspace of approximations* $\Phi_0 \subset \Phi$*,* $\dim \Phi_0 < \infty$*,* $n = 0$*, are specified*;

2. *calculate an approximation* $\boldsymbol{\psi}_n \in \Phi_n$ *such that*

$$\Pi(\boldsymbol{\psi}_n, \boldsymbol{\varphi}) = \langle l, \boldsymbol{\varphi} \rangle \quad \forall\, \boldsymbol{\varphi} \in \Phi_n;$$

3. *estimate the error* using a posteriori estimator of the form $\boldsymbol{\varepsilon}_n(z) = \sum_{K \in \mathcal{T}_n} b_K(z) \boldsymbol{\lambda}_K \in \Phi_n$*, where the coefficients* $\boldsymbol{\lambda}_K$ *satisfy the equation*

$$\Pi(\boldsymbol{\varepsilon}_n, \mathbf{b}_m) = \langle \mathcal{R}_{i+1/2}, \mathbf{b}_m \rangle, \quad m = 1, 2, 3,$$

where supp $b_K = K$, and, for example, for $K = K_{i+1/2} = (z_i, z_{i+1})$ it is assumed that

$$b_K(z) := 4\, \frac{(z - z_i)(z_{i+1} - z)}{(z_{i+1} - z_i)^2} \quad \forall z \in K_{i+1/2},$$

$$\mathbf{b}_1 = [b_K, 0, 0]^T, \quad \mathbf{b}_2 = [0, b_K, 0]^T, \quad \mathbf{b}_3 = [0, 0, b_K]^T.$$

The set of vectors $\{\boldsymbol{\lambda}_K\}_{K \in \mathcal{T}_n}$ approximates the pointwise errors of the displacement vectors at the midpoints of the finite elements of the partition, whilst the set of energy norms $\{\eta_K\}_{K \in \mathcal{T}_n} = \{\|b_K \boldsymbol{\lambda}_K\|_\Pi\}_{K \in \mathcal{T}_n}$ describes their integral characteristics — the distribution of the AEE indicators on the elements of the moving mesh $\mathcal{T}_n$ and its norm

$$\|\boldsymbol{\varepsilon}_n\|_\Pi = \left(\sum_{K \in \mathcal{T}_n} \|b_K \boldsymbol{\lambda}_K\|_\Pi^2 \right)^{1/2};$$

4. *Identify the finite elements* from $\mathcal{T}_n$ that are subject to reconstruction, more precisely: *determine the set of elements* $\mathcal{R}^n = \{K\} \subset \mathcal{T}_n$ *such that*

$$m_K := E\left[\frac{100\sqrt{N_n}\|b_K\boldsymbol{\lambda}_K\|_\Pi}{\|\boldsymbol{\psi}_n\|_\Pi \cdot tol}\right] \geq 1. \tag{6.2}$$

Here, $N_n = \mathrm{card}(\mathcal{T}_n)$, $E(x)$ computes the integer part of the real number $x \geq 0$, and tol is the prescribed tolerance in percent (e.g., $tol = 1$ for a 1% accuracy requirement, consistent with the percentage-based error measures δ_n, r_n). The natural number m_K indicates by how many times the error indicator exceeds its permissible value on the finite element.

5. *Terminate the calculation process* if the set $\mathcal{R}^n$ is empty, $\mathrm{card}(\mathcal{R}^n) = 0$, and prepare tables, graphs, etc., summarising the results of the computational experiment.

6. *Modify the finite elements* of the set $\mathcal{R}^n$, if it is non-empty, $\mathrm{card}(\mathcal{R}^n) \geq 1$. In this case, each finite element $K = K_{i+1/2} \in \mathcal{R}^n$ is assigned m_K additional points with coordinates

$$\alpha_k := z_i + \frac{h_{i+1/2}}{m_K + 1}\, k, \quad k = 1, \ldots, m_K,$$

which form the nodes of its partition into $(m_K + 1)$ parts of equal length. By replacing each $K \in \mathcal{R}^n$ with its parts in the partition $\mathcal{T}_n$, we obtain a new locally improved set of finite elements $\mathcal{T}_{n+1}$, and thus the possibility of constructing an improved subspace of approximations $\Phi_{n+1} \subset \Phi$. It is known [13] that the embedding of spaces $\Phi_n \subset \Phi_{n+1} \subset \Phi$ guarantees the convergence of the approximations constructed on them; therefore, by setting $n := n + 1$, we return to step 1 to continue the calculations according to our algorithm.

7 Results of numerical experiments

Here we analyse the reliability and computational efficiency of the algorithm for constructing a convergent sequence of approximate solutions to problem (3.1)–(3.3), found on a sequence of nested subspaces of finite element approximations; see Section 5 of this article.

7.1 Shell with boundary layers

We continue our consideration of the problem of an axisymmetric static load on a cylindrical shell, the stress-strain state of which is analysed within the framework of Timoshenko's theory. As in a recent article [13], we assume that the geometric and physical parameters of this specimen are as follows: thickness $t = 0.0025\,\mathrm{m}$, radius of the mid-surface $R = 0.5\,\mathrm{m}$, meridian length $L = 1\,\mathrm{m}$, external surface load $f_u = 0\,\mathrm{Pa}$, $f_w = -1000\,\mathrm{Pa}$, $f_\gamma = 0\,\mathrm{Pa}$, Young's modulus $E = 10^9\,\mathrm{Pa}$ and Poisson's ratio $\nu = 0.3$; its ends $z = 0$ and $z = L$ are rigidly clamped.

Under these conditions, the similarity criterion [12] takes the value

$$\mathcal{N} = \frac{1}{2\sqrt{6\nu}}\frac{R}{L}\frac{t}{L} \cong 0.0005,$$

which indicates singular perturbation of the stress-strain state of such a shell model in the neighbourhood of its ends. In this case, the use of piecewise linear finite element approximations allows the approximate solution to this problem to be computed with an acceptable error level of $tol = 1\,\%$ on a uniform subdivision of the interval $\Omega = [0, L]$ with 2560 finite elements. The computational cost of computing such an approximate solution amounts to $N_\Sigma = 3 \cdot 2560 = 7680$ algebraic equations. Figs. 7.1 and 7.2 illustrate the reproduced complex boundary-layer structures of the displacement vector and its derivative for the obtained approximation.

The displacement modulus $|\boldsymbol{\psi}_h|$ (Fig. 7.1) is strongly localised near the clamped ends and decays rapidly towards the shell interior, confirming the singular perturbation character of the problem. Modulus $|d\boldsymbol{\psi}_h/dz|$ (Fig. 7.2) exhibits considerably sharper peaks at the boundaries, reflecting the steep gradients that make uniform mesh refinement computationally prohibitive for this class of problems.

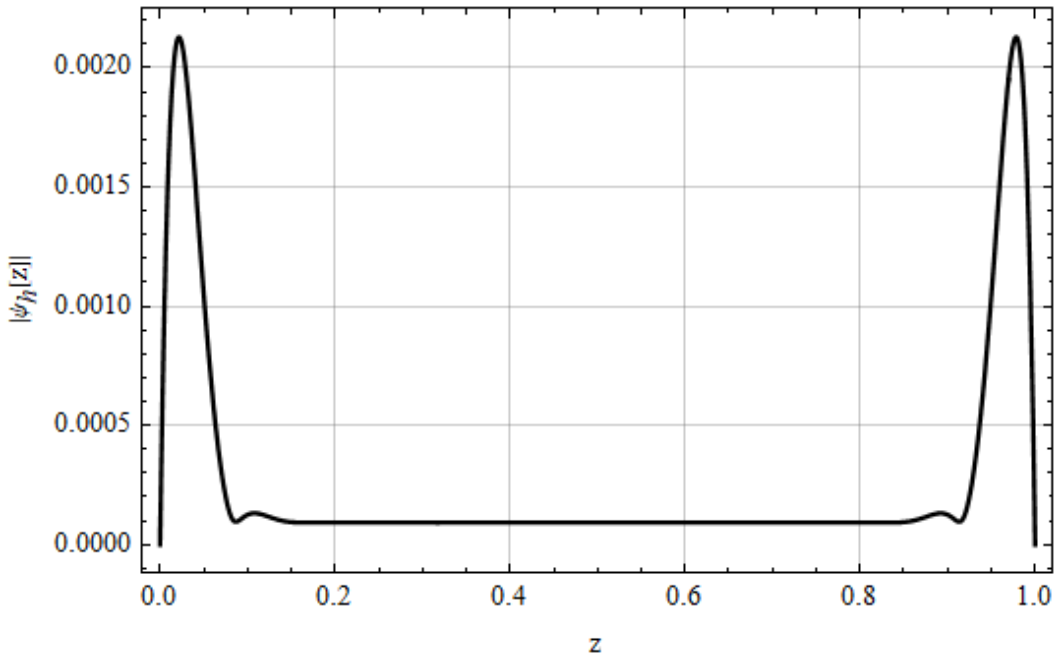

Fig. 7.1. Modulus of the vector of generalised shell displacements $|\boldsymbol{\psi}_h(z)|, \operatorname{card}(\mathcal{T}_n) = 2560$.

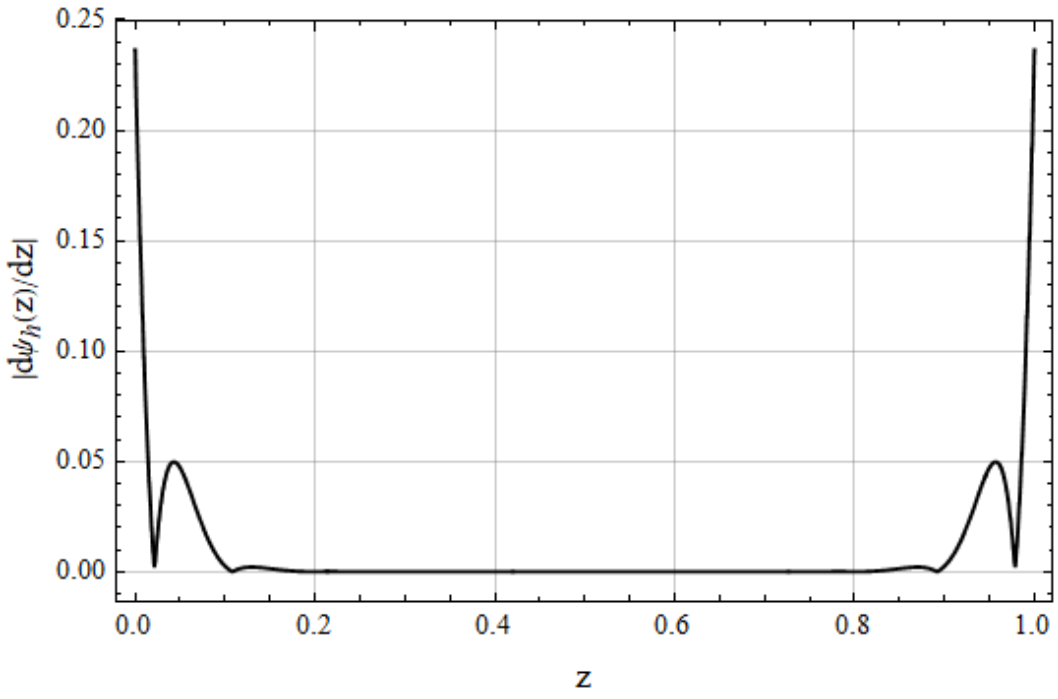

Fig. 7.2. Modulus of the derivative of the vector of generalised shell displacements $\left|\dfrac{d}{dz}\boldsymbol{\psi}_h(z)\right|$, $\operatorname{card}(\mathcal{T}_n) = 2560$.

With this in mind, we will test the h-adaptive algorithm from Section 5 using a scenario that involves answering the following questions:

(i) estimate *the computational cost* required to achieve an approximation error of $tol = 1\,\%$, taking into account the number of local grid refinement steps performed and the total number of FEM algebraic equations formed and solved;

(ii) calculate *the convergence rates* of the sequence of generated approximations according to rule (5.2) (a priori error estimates suggest that, in the case of piecewise linear finite element approximations, the order of convergence of errors in the energy norm is equal to one);

(iii) the effect of *the irregularity of the finite element mesh* χ_n, defined in (5.3), on the stability of the approximations;

(iv) *the quality index of the estimator* I_n defined in (5.4), how close it is to one and how accurately it allows the calculation of two-sided error estimates (5.5);

(v) let a given natural number $M_{\max} \geq 1$ limit the number of parts of the uniform subdivision of a finite element of the mesh in the following way: if, for some $K \in \mathcal{R}^n$, the subdivision number m_K calculated according to criterion (6.2) exceeds the value $M_{\max}$, then set $m_K \equiv M_{\max}$, in other words,

$$m_K := \min\{m_K, M_{\max}\} \quad \forall\, K \in \mathcal{R}^n. \tag{7.1}$$

Assess *the influence of the parameter* $M_{\max} \geq 1$ on the performance and computational cost of our h-adaptive FEM algorithm.

The computation of the true relative error r_n (5.1) and the estimator efficiency index I_n (5.4) requires knowledge of the exact solution and its energy norm $\|\boldsymbol{\psi}\|_\Pi$. To this end, the exact solution $\boldsymbol{\psi}$ of the boundary value problem (2.4), (2.6) was obtained analytically using the eigenvalue method of [7]. The resulting exact solution yields the energy norm $\|\boldsymbol{\psi}\|_\Pi = 0.92972$.

Table 7.1 presents the results of calculating an approximation of the desired accuracy to the solution of the above-mentioned problem, provided that the algorithm described in Section 5 is used with an admissible twofold refinement ($M_{\max} = 1$) of finite elements in accordance with criterion (7.1). The total computational cost of finding such an approximation involves the formulation and solution of $N_\Sigma = 3 \cdot 1780 = 5\,340$ algebraic equations, which amounts to approximately 0.7 of the cost incurred for computations with uniform finite element mesh refinement.

Table 7.1. Convergence of h-adaptive piecewise linear approximations of the displacement vector. Maximum permissible refinement of the finite element $M_{\max} = 1$.

n	N_n	χ_n	$\|\boldsymbol{\psi}_n\|_\Pi$	$\|\boldsymbol{\varepsilon}_n\|_\Pi$	$\delta_n, \%$	$r_n, \%$	$\eta_n, \%$	p_n
0	20	1	0.87232	0.187	21.5	100.0	36.9	—
1	38	2	0.89609	0.159	17.7	23.0	27.6	0.26
2	58	4	0.91219	0.130	14.2	18.8	19.6	0.48
3	86	8	0.92225	0.098	10.6	14.7	12.6	0.72
4	126	16	0.92726	0.063	6.8	10.3	7.2	1.16
5	190	32	0.92904	0.035	3.7	6.1	3.8	1.44
6	292	64	0.92954	0.018	1.9	3.3	2.0	1.52
7	438	128	0.92967	0.010	1.1	1.7	1.1	1.53
8	532	256	0.92969	0.007	0.7	0.8	0.7	2.02

In this table: $n \geq 0$ is the refinement step number, $N_n = \mathrm{card}(\mathcal{T}_n)$ the number of finite elements in the mesh $\mathcal{T}_n$, $\chi_n = \chi(\mathcal{T}_n)$ its irregularity, errors $\delta_n = \frac{\|\boldsymbol{\varepsilon}_n\|_\Pi}{\|\boldsymbol{\psi}_n\|_\Pi}100\%$, $r_n = \frac{\|\boldsymbol{\psi}-\boldsymbol{\psi}_n\|_\Pi}{\|\boldsymbol{\psi}_n\|_\Pi}100\%$, $\eta_n = \frac{\|\boldsymbol{\psi}_{n+1}-\boldsymbol{\psi}_n\|_\Pi}{\|\boldsymbol{\psi}_n\|_\Pi}100\%$; the order of convergence $p_n = \frac{\ln\|\boldsymbol{\varepsilon}_{n-1}\|_\Pi - \ln\|\boldsymbol{\varepsilon}_n\|_\Pi}{\ln[\mathrm{card}(\mathcal{T}_n)] - \ln[\mathrm{card}(\mathcal{T}_{n-1})]}$. The permissible relative error of the approximation is $tol = 1\%$.

Interestingly, from step to step of refinement, the increase in the number of finite elements is $\frac{N_n}{N_{n-1}} \cong 1.5$ times (with an expected increase in irregularity $\chi_n = 2$); thus, the division of elements occurred only (locally) on a portion of the grid elements, with some of them remaining untouched until the completion of the calculations. The remaining indicators in the table demonstrate a stable monotone behaviour of the sequences of approximation characteristics, among which the increase in the order of convergence of the approximations to $p_8 \geq 2$ should be highlighted. This fact confirms the numerically observed high convergence rate of the developed FEM even in the process of analysing models of singularly perturbed problems. Finally, we note that the intelligent refinement of the finite element mesh structure employed here has enabled the calculation of an approximation of the displacements of a shell of a given class on an irregular mesh with $N_n = 532$ finite elements.

Table 7.2 presents the results of calculations carried out to determine the sensitivity of our adaptation algorithm to the performance of approximation generation for different values of the constraint parameter $M_{\max} = 1, 2, \ldots$, and to establish whether there exists a practically efficient value of $M^*_{\max} \geq 1$ for which the process of finding an approximation of the desired quality is performed with reduced use of computational resources. For such an $M^*_{\max}$, the computation of approximations of the required accuracy should ensure the stability and convergence of the sequence of generated h-adaptive approximations with a priori predictable convergence orders (in our case equal to one).

Table 7.2. Effect of the finite element refinement parameter $M_{\max} \geq 1$ on the total number of refinement steps for approximations.

$M_{\max}$	n	N_n	χ_n	$\|\boldsymbol{\psi}_n\|_\Pi$	$\|\boldsymbol{\varepsilon}_n\|_\Pi$	$\delta_n, \%$	$r_n, \%$	$\eta_n, \%$	p_n	N_Σ	I_n
1	8	532	256	0.9297	0.0066	0.71	0.72	0.78	2.02	5340	1.01
2	5	524	243	0.9297	0.0070	0.74	0.76	1.37	1.76	3642	1.02
3	4	522	256	0.9297	0.0067	0.72	0.73	1.81	1.87	3150	1.01
4	4	566	500	0.9297	0.0062	0.67	0.68	0.83	1.94	3876	1.02
5	3	522	216	0.9297	0.0071	0.77	0.78	3.33	1.85	2592	1.01
6	3	582	343	0.9297	0.0062	0.67	0.68	2.46	1.88	2952	1.02
7	3	610	512	0.9297	0.0060	0.65	0.66	1.91	1.88	3210	1.02
8	3	642	567	0.9297	0.0057	0.61	0.62	1.46	1.84	3480	1.02
9	3	636	500	0.9297	0.0058	0.62	0.64	1.17	1.87	3624	1.02
10	3	620	484	0.9297	0.0059	0.63	0.64	0.92	2.02	3738	1.02
11	2	498	144	0.9297	0.0092	0.99	1.00	9.23	1.72	1986	1.01
12	2	530	169	0.9297	0.0082	0.88	0.89	8.73	1.77	2106	1.01
13	2	552	196	0.9297	0.0074	0.80	0.81	8.29	1.81	2190	1.01
14	2	574	225	0.9297	0.0069	0.74	0.75	7.89	1.83	2274	1.01
15	2	596	256	0.9297	0.0065	0.70	0.70	7.53	1.85	2358	1.01
16	2	616	289	0.9297	0.0061	0.65	0.66	7.21	1.87	2436	1.01
17	2	636	324	0.9297	0.0058	0.63	0.64	6.91	1.87	2514	1.01
25	2	700	598	0.9297	0.0053	0.57	0.58	5.32	1.86	2802	1.01

In this table: n is the total number of refinement steps, $N_n = \mathrm{card}(\mathcal{T}_n)$ the number of finite

elements in the mesh at the final refinement step, its irregularity χ_n, convergence orders p_n, computational costs N_Σ (total algebraic equations) and the AEE efficiency index $I_n = \frac{\|\boldsymbol{\psi}-\boldsymbol{\psi}_n\|_\Pi}{\|\boldsymbol{\varepsilon}_n\|_\Pi}$. Here $\delta_n = \frac{\|\boldsymbol{\varepsilon}_n\|_\Pi}{\|\boldsymbol{\psi}_n\|_\Pi}100\%$, $r_n = \frac{\|\boldsymbol{\psi}-\boldsymbol{\psi}_n\|_\Pi}{\|\boldsymbol{\psi}_n\|_\Pi}100\%$, $\eta_n = \frac{\|\boldsymbol{\psi}_{n+1}-\boldsymbol{\psi}_n\|_\Pi}{\|\boldsymbol{\psi}_n\|_\Pi}100\%$ are error estimates calculated at the final refinement step. The permissible relative error of approximation is $tol = 1\%$.

In view of the data in this table, it is worth noting:

(i) an increase in the values of the step size parameter $M_{\max} \geq 1$ leads to a rapid monotonic decrease in the number of steps required to improve the approximation to the desired quality, from 8 steps for $M_{\max} = 1$, to 3 steps for $M_{\max} = 5$, and stops at 2 refinement steps for all $M_{\max} \geq 11$;

(ii) *the computational cost* (measured by the total number of equations solved N_Σ) required to achieve the desired approximation quality was maximum $N_\Sigma = 5340$ for calculations with $M_{\max} = 1$, fluctuated within the range $2592 \leq N_\Sigma \leq 3738$ for values of $5 \leq M_{\max} \leq 10$ and reached a minimum $N_\Sigma = 1986$ at $M_{\max} = 11$;

(iii) calculations using the parameter $M_{\max} = 11$ yielded *noteworthy results*: the smallest number of solved equations $N_\Sigma = 1986$, calculated on the least irregular mesh $\chi(\mathcal{T}^*) = \frac{\max_{K\in\mathcal{T}^*} h_K}{\min_{K\in\mathcal{T}^*} h_K} = 144$ with the (smallest) number of finite elements $\mathrm{card}(\mathcal{T}^*) = 498$; the approximations calculated from $M_{\max} > 11$ were characterised by small fluctuations in the values of the parameters: $N_\Sigma \in [2106, 2802]$, $\mathrm{card}(\mathcal{T}^m) \in [530, 700]$, $\chi(\mathcal{T}^m) \in [196, 600]$, confirming that an increase in the parameter $M_{\max}$ adds nothing significant to the search for optimisation of computational costs;

(iv) the order of convergence of the approximate error values (AEE) p_n was almost independent of the value of $M_{\max}$, consistently taking values from the interval $[1.7, 2.0]$, which indicates a numerically observed high convergence rate of our local adaptation algorithm;

(v) *the calculated values of the efficiency index* I_n consistently showed values no greater than 1.02, which indicates the high quality and reliability of the constructed AEE. Moreover, for the data from Table 7.2 and $I_n = 1.02$, formula (5.5) establishes the lower and upper bounds of the errors of the form

$$0.98 \cdot \|\boldsymbol{\varepsilon}_n\|_\Pi \leq \|\boldsymbol{\psi} - \boldsymbol{\psi}_n\|_\Pi \leq 1.02 \cdot \|\boldsymbol{\varepsilon}_n\|_\Pi.$$

7.2 Shell with boundary and internal layers

We continue the analysis of the properties of our adaptive FEM scheme by considering the axisymmetric static equilibrium problem for a cylindrical shell with rigidly clamped ends under a local surface load described by the force vector

$$f_u = 0, \quad f_w(z) = \begin{cases} 0, & 0.0 \leq z \leq 0.4, \\ -10^5(z-0.4)(0.6-z)\,\mathrm{Pa}, & 0.4 \leq z \leq 0.6, \\ 0, & 0.6 \leq z \leq 1.0, \end{cases} \quad f_\gamma = 0. \tag{7.2}$$

The geometric and physical parameters are the same as in the previous example: thickness $t = 0.0025\,\mathrm{m}$, mid-surface radius $R = 0.5\,\mathrm{m}$, meridian length $L = 1\,\mathrm{m}$, Young's modulus $E = 10^9\,\mathrm{Pa}$, Poisson's ratio $\nu = 0.3$; ends $z = 0$ and $z = L$ are rigidly clamped.

Under these conditions, the similarity criterion [12] takes the same value $\mathcal{N} \cong 0.0005$, which now signals singular perturbation of the stress-strain state both near the clamped ends *(boundary layers)* and near the load-discontinuity points $z = 0.4$ and $z = 0.6$ *(internal layers)*. The presence of mixed-type layers further complicates the numerical modelling of this problem by standard FEM algorithms.

The goal is to assess the efficiency and reliability of our adaptive scheme for computing an approximation with a prescribed tolerance $tol \le 3\,\%$, starting from a coarse uniform mesh $\mathcal{T}_0$ with $N_0 = \mathrm{card}(\mathcal{T}_0) = 10$ elements and refinement parameter $M_{\max} = 5$, which was identified in Section 7 as the value yielding the lowest computational cost for this class of problems.

Since no exact solution is available for this loading case, the efficiency index of the estimator is computed via the surrogate rule

$$I_n := \frac{\|\boldsymbol{\psi}_{n+1} - \boldsymbol{\psi}_n\|_{\Pi}}{\|\boldsymbol{\varepsilon}_n\|_{\Pi}}. \tag{7.3}$$

Three local mesh-refinement steps were sufficient to achieve the required accuracy. The computed characteristics of the approximations are given in Table 7.3.

Table 7.3. Convergence of h-adaptive piecewise linear approximations under local load (7.2) with $M_{\max} = 5$, $N_0 = 10$, $\chi_0 = 1$, $tol \le 3\,\%$.

n	N_n	χ_n	$\|\boldsymbol{\psi}_n\|_{\Pi}$	$\|\boldsymbol{\varepsilon}_n\|_{\Pi}$	$\delta_n, \%$	p_n	$\eta_n, \%$	I_n
0	10	1	0.73641	0.364233	49.46	—	64.69	1.31
1	54	2	0.96556	0.264116	27.35	1.22	32.23	1.18
2	172	12	1.02013	0.083922	8.23	1.23	8.92	1.08
3	450	72	1.02418	0.025510	2.49	1.36	—	—

In addition to the stable convergence orders $p_n \ge 1.2$, we note the monotone decrease of the efficiency indices towards unity. This allows us to establish, at the final refinement step, the two-sided bounds

$$0.93\,\|\boldsymbol{\varepsilon}_2\|_{\Pi} \le \|\boldsymbol{\psi} - \boldsymbol{\psi}_2\|_{\Pi} \le 1.08\,\|\boldsymbol{\varepsilon}_2\|_{\Pi}.$$

The AEE $\mathcal{E}_n(z)$, the distributions of its indicators, and the finite element sizes $\mathcal{H}_n(z)$ at each refinement step, represented as piecewise constant functions

$$\mathcal{E}_n(z) := \sum_{i=1}^{N_n} \|\boldsymbol{\varepsilon}_{i+1/2}\|_{\Pi}\, \varrho_{i+1/2}(z), \quad \mathcal{H}_n(z) := \sum_{i=1}^{N_n} h_{i+1/2}\, \varrho_{i+1/2}(z), \quad \varrho_{i+1/2}(z) := \begin{cases} 0, & 0 \le z \le z_i, \\ 1, & z_i \le z \le z_{i+1}, \\ 0, & z_{i+1} \le z \le L \end{cases}$$

are presented in Figs. 7.3–7.6.

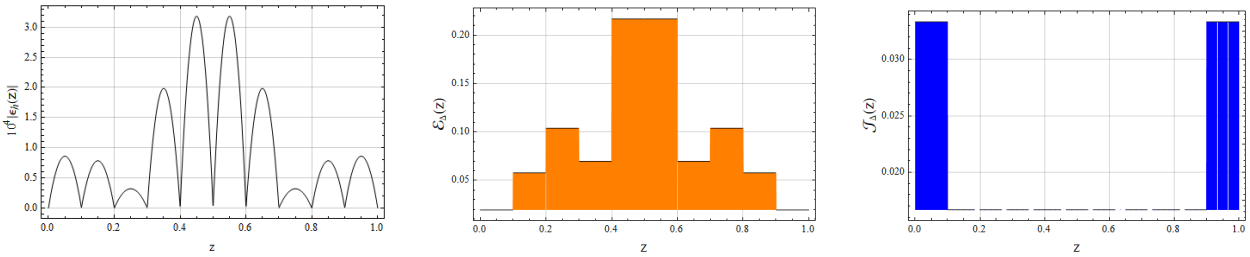

Fig. 7.3. Left: AEE $\mathcal{E}_0(z)$ on initial mesh $N_0 = 10$; centre: AEE indicator distribution; right: element sizes of refined mesh $\mathcal{T}_1$, $N_1 = 54$, $\chi_1 = 2$.

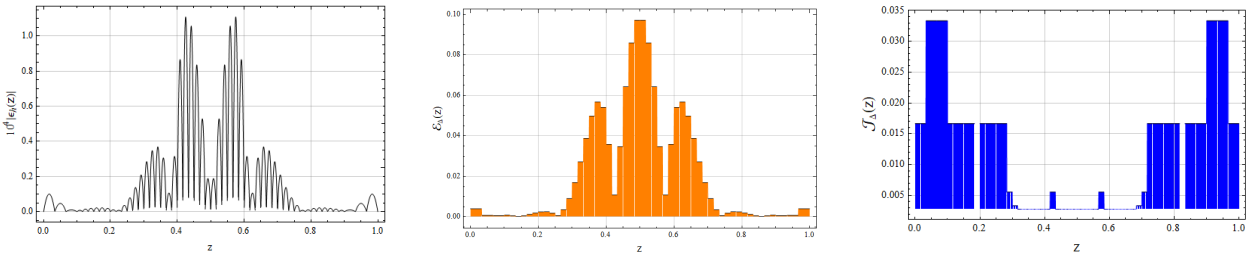

Fig. 7.4. Left: AEE $\mathcal{E}_1(z)$ on mesh $N_1 = 54$; centre: AEE indicator distribution; right: element sizes of refined mesh $\mathcal{T}_2$, $N_2 = 172$, $\chi_2 = 12$.

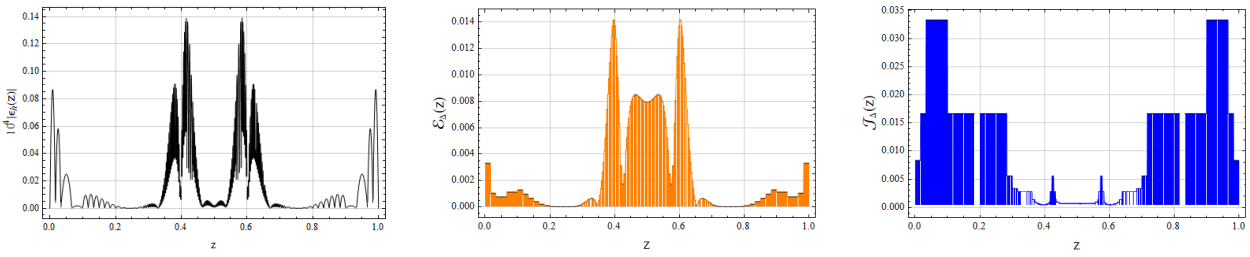

Fig. 7.5. Left: AEE $\mathcal{E}_2(z)$ on mesh $N_2 = 172$; centre: AEE indicator distribution; right: element sizes of refined mesh $\mathcal{T}_3$, $N_3 = 450$, $\chi_3 = 72$.

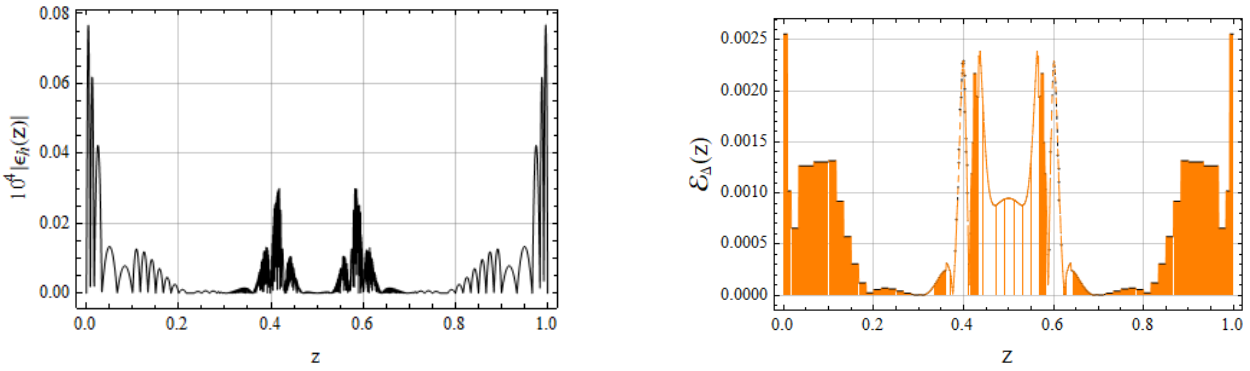

Fig. 7.6. Left: AEE $\mathcal{E}_3(z)$ on final mesh $N_3 = 450$, $\chi_3 = 72$; right: AEE indicator distribution.

Already on the coarse initial mesh (Fig. 7.3), the estimator indicators correctly identify dominant approximation errors on the loaded segment $0.4 \le z \le 0.6$ and drive the generation of a non-uniform mesh subject to the $M_{\max} = 5$ subdivision limit. Some of the longest elements (of length 0.033 m) remain unchanged in subsequent refinement steps, confirming the high quality of the AEE. The final figure of this series (Fig. 7.6) shows that only at the last refinement step does the estimator simultaneously detect features of comparable magnitude in both the internal and boundary layers.

The stress resultants N_u, N_w, N_{13}, M_γ computed from the final approximation are shown in Fig. 7.7.

The shear force $N_{13}(z)$ and bending moment $M_\gamma(z)$ exhibit a complex structure near the internal layers; notably, $N_{13}(z)$ is the only resultant that also responds to the boundary layers through a growth in its values near the clamped ends.

The corresponding generalised displacement components $u(z)$, $w(z)$, $\gamma(z)$ and their modulus $|\boldsymbol{\psi}_3(z)|$ are shown in Fig. 7.8. The graphs confirm that the displacement field exhibits pronounced features only in the neighbourhood of the internal layers, while the influence of the boundary layers manifests primarily in the stress-resultant fields.

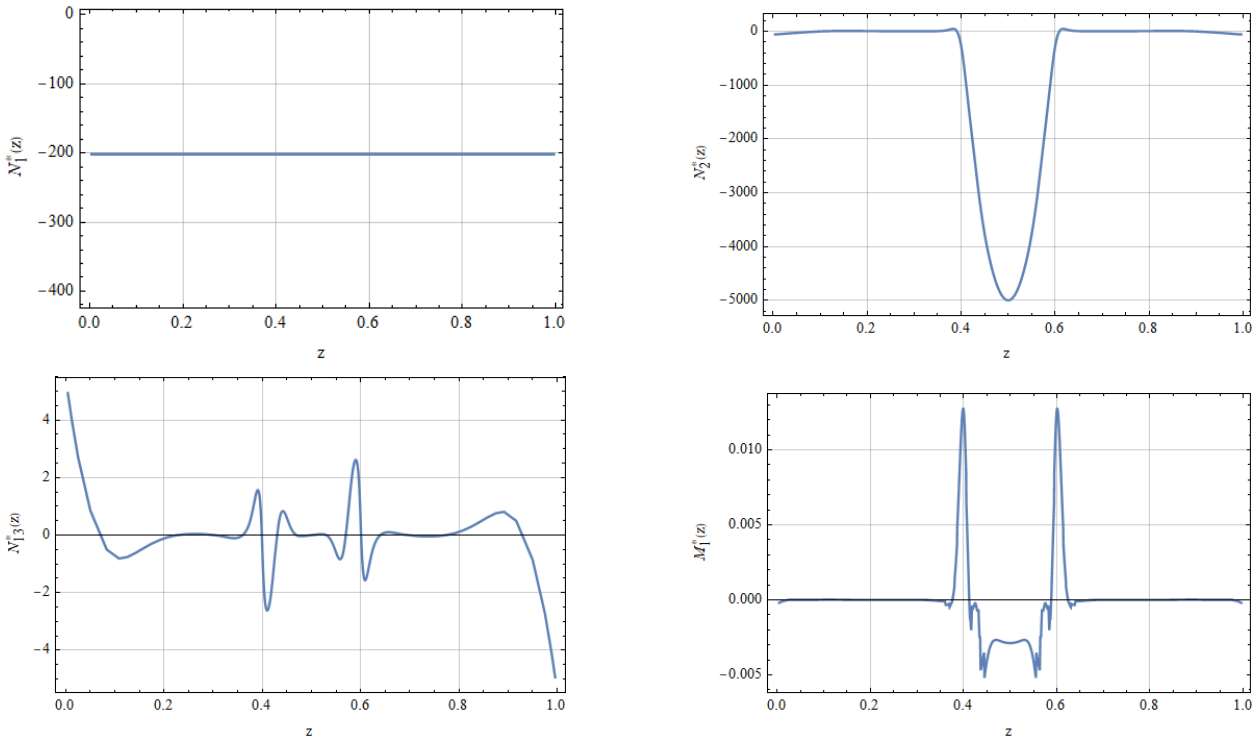

Fig. 7.7. Stress resultants $N_u(z)$, $N_w(z)$, $N_{13}(z)$, $M_\gamma(z)$ at the final refinement step $n = 3$.

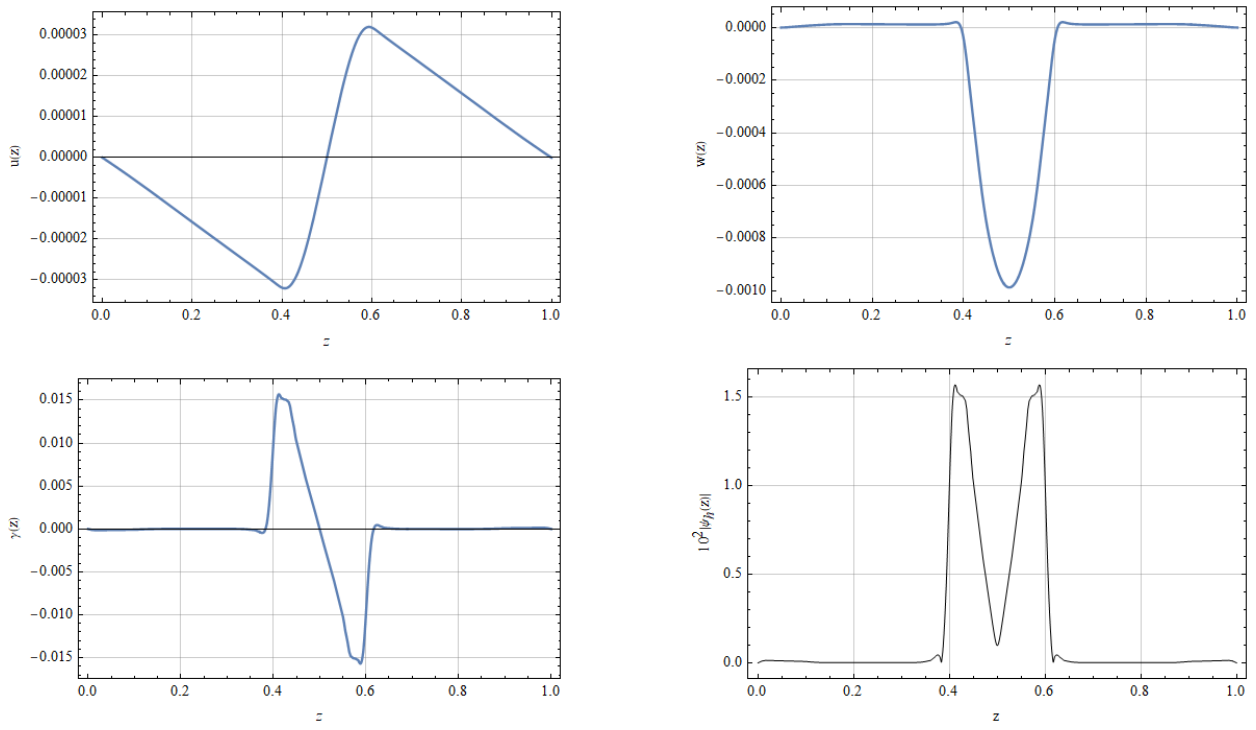

Fig. 7.8. Generalised displacement components $u(z)$, $w(z)$, $\gamma(z)$ and modulus $|\psi_3(z)|$ at the final refinement step $n = 3$.

8 Conclusions and final remarks

Here we analyse the reliability and computational efficiency of the h-adaptive algorithm for the construction of a convergent sequence of approximate solutions to problems (3.1)–(3.3), generated by a sequence of nested subspaces of finite element approximations. At each step of this refinement procedure, we obtain *the best* (in terms of the energy norm $\|\cdot\|_\Pi$) *approximation* $\boldsymbol{\psi}_n$ to the true solution of the problem *by elements of the approximation subspace* Φ_n. It is on this very distinctive property that the a posteriori error estimator for piecewise linear finite element approximations is based — on each finite element of the computational grid, its indicator functions compute *the best approximations to the true error*. Thus, the technology proposed here provides a firm basis for solving complex, in particular singularly perturbed, problems in shell theory.

In view of the computational experiments carried out, the multiple subdivision of finite elements provides a significant advantage in the implementation of the h-adaptive FEM scheme, which ultimately leads to a significant reduction in the steps of local refinement of the mesh structure, together with a reduction in the computational cost of finding an approximation of the solution to the problem with a predefined acceptable error.

At the same time, the example of a singularly perturbed problem we have considered demonstrates the existence of a practically efficient number of admissible subdivisions of the element, the use of which significantly reduces the computational cost of calculating approximations of the desired accuracy.

It is established that for all values of the refinement parameter $M_{\max}$, the h-adaptive FEM algorithm consistently demonstrated high convergence rates with efficiency indices close to unity.

Declarations

Conflict of Interest.
The authors have no conflict of interest to declare that are relevant to the content of this article.
Funding.
This study was not supported by any sponsor or funder.
Author Contributions.
Authors contributed equally to the research and preparation of this article.

Additional information

H. S. is a member of the Editorial Board for JANA. The paper was handled by another Editor and has undergone a rigorous peer review process. H. S. was not involved in the journal's peer review, or decisions related to this manuscript.

References

1. Abramov, E., Lipina, O., Shynkarenko, G., Yamelynets, A.: Piecewise-linear approximations of the h-adaptive finite element method for one-dimensional boundary value problems. Bulletin of Lviv University. Series on Applied Mathematics and Informatics. **11**, 3–18 (2006). (in Ukrainian). 236
2. Ainsworth, M., Oden, J. T.: A posteriori error estimation in finite element analysis. John Wiley & Sons, New York (2000). doi:10.1002/9781118032824 3, 236, 238
3. Babuška, I., Rheinboldt, W.: Error estimates for adaptive finite element computations. SIAM J. Numer. Analysis. **15**, 736–754 (1978). 235
4. Babuška, I., Strouboulis, T.: The finite element method and its reliability. Oxford University Press, Oxford (2001). doi:10.1093/oso/9780198502760.001.0001 236

5. Babuška, I., Whiteman, J. R., Strouboulis, T.: Finite Elements: An Introduction to the Method and Error Estimation. Oxford University Press, Oxford (2011). 236
6. Chamoin, L., Legoll, F.: An introductory review on a posteriori error estimation in finite element computations. SIAM Review. **65** (4), 917–1197 (2023). doi:10.1137/21M1464841 236
7. Ghannad, M., Zamani Nejad, M.: Elastic analysis of pressurized thick hollow cylindrical shells with clamped-clamped ends. Mechanika. **85** (5), 11–18 (2010). doi:10.5755/j02.mech.15963. 244
8. Gorlach, V. M., Lazarenko, Yu. V.: Modification of the h-adaptation algorithm for solving one-dimensional boundary value problems using the FEM. Contemporary Problems in Applied Mathematics and Informatics: Proc. XVII All-Ukrainian Scientific Conf. Lviv: LNU Publishing Centre, p. 38 (2011). (in Ukrainian). 236
9. Grygorenko, Y. M., Savula, Y. G., Mukha, I. S.: Linear and non-linear problems of elastic deformation of complex-shaped shells and methods for their numerical solution. International applied mechanics. **36** (8), 979–1000 (2000). (in Ukrainian). 236
10. Savula, Y. G., Fleishman, N. P.: Calculation and optimisation of shells with carved mid-surfaces. Vyshcha Shkola, Lviv (1989). (in Ukrainian). 236
11. Segeth, K.: A review of some a posteriori error estimates for adaptive finite element methods. Math. Comput. Simul. **80**, 1589–1600 (2010). doi:10.1016/j.matcom.2008.12.019 3, 236
12. Shynkarenko, H., Malashnyak, P.: Analysis of the h-adaptive finite element method in the problem of the statics of cylindrical shells: I. Correctness of the axisymmetric variational formulation. Physical and Mathematical Modelling and Information Technologies. **40**, 27–36 (2025). (in Ukrainian). doi:10.15407/10.15407/fmmit2025.40.027 237, 238, 242, 246
13. Shynkarenko, H., Malashnyak, P.: Analysis of the h-Adaptive Finite Element Method in Static Problems of Cylindrical Shells: II. Piecewise Linear Approximations and an A Posteriori Error Estimator. Physical and Mathematical Modelling and Information Technologies. **40**, 35–49 (2026). (in Ukrainian). doi:10.15407/fmmit2026.42.035 238, 240, 242
14. Trushevsky, V. M., Shynkarenko, G. A., Shcherbina, N. M.: The finite element method and artificial neural networks. Theoretical aspects and applications. Ivan Franko National University of Lviv Publishing Centre, Lviv (2014). (in Ukrainian). 236
15. Verfürth, R.: A Review of A Posteriori Error Estimates and Adaptive Mesh-Refinement Techniques. Wiley-Teubner, New York (1996). 236
16. Verfürth, R.: A Posteriori Error Estimation Techniques for Finite Element Methods. Oxford University Press, Oxford (2013). doi:10.1093/acprof:oso/9780199679423.001.0001 236
17. Zienkiewicz, O. C., Taylor, R. L., Zhu, J.: The Finite Element Method: Its Basis and Fundamentals. 7th ed., Elsevier, Oxford (2015). 236

Received 08.06.2026
Revised 28.07.2026
Accepted 31.07.2026